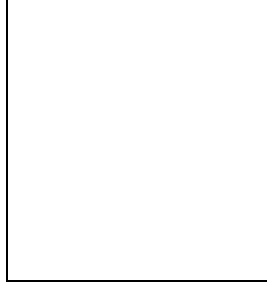


Propagation of UHECRs

Daniel De Marco
Bartol Research Institute, University of Delaware
Newark, DE 19716, U.S.A.



In this general introduction to Ultra High Energy Cosmic Rays (UHECRs) we discuss the propagation of UHE protons and the GZK feature that is expected approaching 10^{20} eV for homogeneously distributed sources. We also briefly present the effects of the propagation on other particles that can play the role of UHECRs. With the help of numerical simulations for the propagation of UHECRs, we show that the GZK feature cannot be accurately determined with the small sample of events with energies $\sim 10^{20}$ eV detected thus far by the largest two experiments, AGASA and HiRes.

1 Introduction

In the past ninety years of cosmic rays research there has been a constant search for the *end of the cosmic-rays spectrum* and it has long been thought that this end would be determined by the highest energy that cosmic accelerators might be able to achieve. Despite the continuous search, no end of the spectrum was found. In 1966, right after the discovery of the cosmic microwave background (CMB), it was understood¹ that high energy protons would interact inelastically with the photons of the CMB and produce pions. For homogeneously distributed sources this would cause a flux suppression, called the *GZK cutoff*: for the first time the end of the cosmic ray spectrum was related to a physical process rather than to speculations on the nature of the accelerators. Moreover, for the first time, the end of the cosmic ray spectrum was predicted to be at a rather well defined energy, around 10^{20} eV, where the so-called photo-pion production starts to be kinematically allowed.

UHECRs can be of various nature and during their propagation over cosmological distances they suffer different kinds of energy losses. In this paper we consider most of the particles that could play the role of UHECRs and we review the processes affecting their propagation. In §2 we discuss the propagation of protons, heavy nuclei, photons and neutrinos. In §3 we show that the two largest experiments operating up to now, AGASA and HiRes, have a too small statistic to

provide a conclusive answer about the presence or absence of the GZK feature in the UHECRs spectrum. We conclude in §4.

2 Propagation of UHECRs in the cosmic photon background

2.1 Protons

There are three sources of energy loss for ultra high energy protons propagating over cosmological distances: the expanding universe redshift, pair production ($p\gamma \rightarrow pe^+e^-$) and photo-pion production ($p\gamma \rightarrow \pi N$), each successively dominating as the proton energy increases.

For protons the most important background is the CMB and the most important process is the photo-pion production in which a nucleon of sufficiently high energy sees, in its reference frame, the photons of the CMB blue-shifted to γ -rays above the threshold energy for photo-pion production, $E_\gamma^{\text{lab,thr}} = m_\pi + m_\pi^2/(2m_N) \simeq 160 \text{ MeV}$. The cross-section for this process has a pronounced resonance just above threshold, corresponding to the production of an intermediate state Δ^+ that immediately decays into a nucleon and a pion, whereas in the limit of high energies it increases logarithmically with $s = m_N^2 + 2m_N E_\gamma^{\text{lab}}$, giving rise to multiple pion production. For a background photon of energy ϵ in the cosmic rest frame, defined as the frame in which the CMB is isotropic, the threshold energy $E_\gamma^{\text{lab,thr}}$ translates into a corresponding threshold for the nucleon energy:

$$E_{\text{thr}} = \frac{m_\pi}{(1 - \cos \theta)\epsilon} \left(m_N + \frac{m_\pi}{2} \right) \simeq 6.8 \cdot 10^{19} \left(\frac{10^{-3} \text{ eV}}{\epsilon} \right) \left(\frac{2}{1 - \cos \theta} \right) \text{ eV}. \quad (1)$$

Typical CMB photon energies are of the order of 10^{-3} eV , giving a threshold value of a few tens of EeV (for a head-on collision).

The interplay of this threshold with the Planck spectrum of the CMB photons produces a very steep, exponential, curve for the interaction length. The combination with the large inelasticity of the photo-pion interaction (the mean inelasticity goes from ~ 0.13 at threshold to ~ 0.5 at high energy, with large fluctuations) creates a very efficient and rapid mechanism to reduce the nucleon energy and makes the universe opaque to nucleons with energy above $\sim 10^{20} \text{ eV}$ on scales above $\sim 100 \text{ Mpc}$. The so-called GZK cutoff is due exactly to this: the flux at earth of nucleons with energy below threshold, say $5 \cdot 10^{19} \text{ eV}$, is due to contributions from (almost) all the universe, from Fig. 1 the loss length at this energy is of the order of 1 Gpc , while doubling the energy the loss length is reduced to 100 Mpc , and only a small portion of the universe contributes to the flux. Thus this change by a factor two in the energy changes the loss length by almost an order of magnitude, which translates in about the same ratio between the flux below $5 \cdot 10^{19} \text{ eV}$ and above 10^{20} eV if the sources have no luminosity evolution and no local overdensity and there is no magnetic field.

Below $\sim 6 \cdot 10^{19} \text{ eV}$ the dominant loss mechanism for protons becomes the production of electron-positrons pairs on the CMB, $p\gamma \rightarrow pe^+e^-$, down to the corresponding threshold:

$$E_{\text{thr}} = \frac{m_e}{\epsilon} (m_N + m_e) \simeq 4.8 \cdot 10^{17} \left(\frac{10^{-3} \text{ eV}}{\epsilon} \right) \text{ eV}. \quad (2)$$

The interaction length for this process is much shorter than the one for pion production, but on the other hand the inelasticity is much lower, $\sim 10^{-3}$. This makes the pair production loss length of the order of Gpc (see Fig. 1). The low inelasticity of pair production allows in calculations to treat this process as a continuous energy loss, whereas the pion production has to be treated as a discrete process due to its large inelasticity.

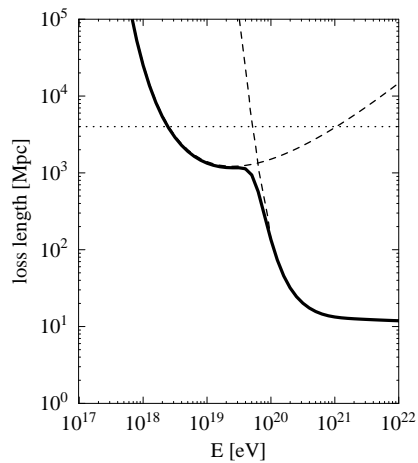


Figure 1: Solid line: loss length for photo-pion and photo-pair production for protons ^{2,3}. The dashed lines report the separate contributions of the two processes. The dotted line shows the redshift losses.

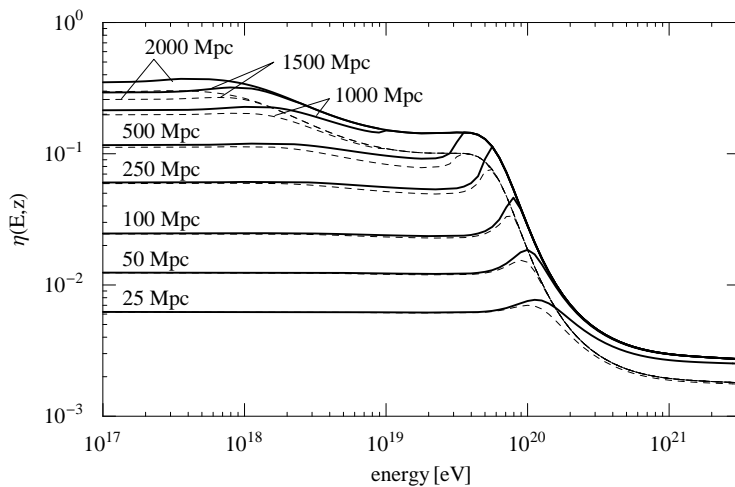


Figure 2: Modification factors as a function of the energy for many-source spectrum with $\gamma = 2.1$ (solid lines) and $\gamma = 2.7$ (dashed lines). The sources are uniformly distributed up to the indicated distances. After Ref. ².

The last important mechanism which dominates near and below the pair production threshold is redshifting due to the expansion of the universe. Fig. 1 shows the loss lengths for pion and pair production as calculated in Ref. ².

It is worth stressing that what has been named the GZK cutoff is in fact a *feature* ⁴ as the shape of the energy spectrum around 10^{20} eV depends on many unknowns. The modifications of the spectrum shape due to the above-mentioned loss processes was first investigated by Berezhinsky and Grigorieva in Ref. ². They calculated the modification factor (basically the observed spectrum divided by the injection spectrum) for a uniform distribution of sources up to a maximum distance d_{\max} . Fig. 2 shows their results for sources without cosmological evolution, $m = 0$, for some values of the maximum distance of the sources. For large d_{\max} , which is the case we are interested in, the spectrum shows a steepening followed by a flattening and then by a suppression. The flattening is due to the interplay between the features produced by the pair and pion production processes and it is an important feature for these spectra since it has a characteristic shape. There are claims that this feature has been observed in the experimental data ², although it is not yet clear if the feature in the data is due to this effect or if it is due to the transition between the galactic and extra-galactic components.

It is important to stress what we said above: what is generically called GZK-cutoff is actually a *feature* as the spectrum does not end at 10^{20} eV (see Fig. 2), but has a flux suppression that depends on many details such as the injection spectrum of cosmic rays, the luminosity evolution of the sources, the local overdensity of sources and the magnetic field strength in the intergalactic medium. As an example, including the luminosity evolution makes the sources at high redshift brighter than the nearby ones and this enhances the flux suppression, while a local overdensity of sources has the opposite effect ⁴; a flatter spectrum produces a lesser attenuation than a steeper one and the strength of the magnetic field in the intergalactic medium can produce many interesting features, see for example Ref. ⁵.

2.2 Heavy Nuclei

For nuclei the situation is slightly different: the dominant loss process above about 10^{19} eV is photodisintegration in the CMB and IR background (IRB) due to the giant dipole resonance,

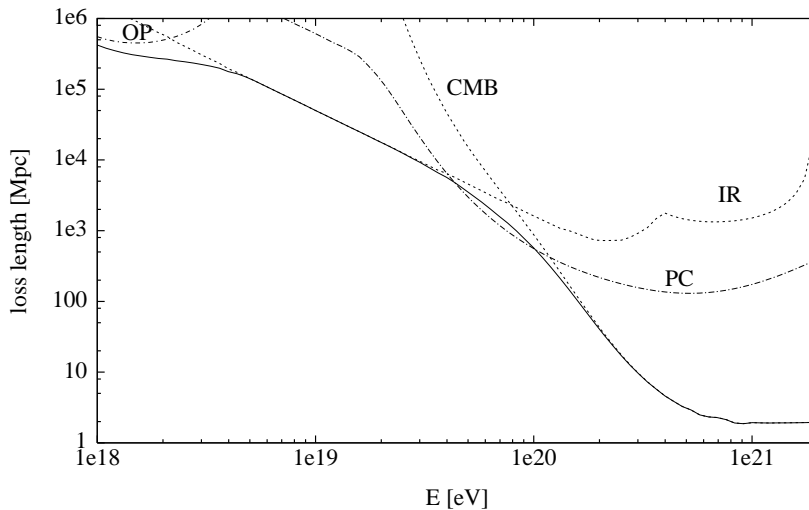


Figure 3: Effective energy loss length for Fe photodisintegration off microwave (CMB), infrared (IR) and optical (OP) photons, as well as the total one (solid line) and the pair production loss length (PC). From Ref. ⁷.

followed at lower energy by the pair production. The photo-pion production process is negligible, except for light nuclei at very high energies ^{6,7}. Indeed, for a nucleus of mass number A and charge Z , the energy loss length for pion production is roughly the same one of a nucleon with identical Lorentz factor. This is due to the fact that the cross section for pion production is approximately proportional to the mass number A , while the inelasticity is proportional to $1/A$. For pair production we got a different behavior because, while the inelasticity is proportional to $1/A$ as before, the cross section is proportional to Z^2 resulting in an energy loss length lower by a factor A/Z^2 with respect to a proton with the same Lorentz factor. Since $Z \sim A/2$, the ratio of the photo-pair and photo-pion production increases roughly linearly with Z ⁸.

The cross sections for photodisintegration $\sigma_{A,i}(\epsilon')$ contains essentially two regimes depending on ϵ' , the photon energy in the nucleus rest frame. At $\epsilon' < 30$ MeV there is the domain of the giant dipole resonance and the disintegration proceeds mainly by the emission of one or two nucleons. At higher energies, the cross section is dominated by multi-nucleon emission for heavy nuclei and is approximately flat up to $\epsilon' \sim 150$ MeV. A useful quantity to estimate the energy loss rate by photodisintegration is given by the effective rate:

$$R_A^{\text{eff}} = \frac{dA}{dt} = \sum_i iR_{A,i}. \quad (3)$$

For photodisintegration, the average fractional energy loss results equal to the fractional loss in mass number of the nucleus, $E^{-1}dE/dt = A^{-1}dA/dt$, because the nucleon emission is isotropic in the rest frame of the nucleus. Therefore during the photodisintegration process the Lorentz factor of the nucleus is conserved, unlike the cases of pair and pion production which involve the creation of new particles that carry away energy. The energy loss time for photodisintegration is then A/R_A^{eff} . Fig. 3 shows separately the different contributions to this quantity from CMB, IR and optical photons for Fe nuclei, together with the total one (solid line) and the pair creation loss length.

It is apparent that the optical background has no relevant effect, that the IR one dominates the photodisintegration processes below 10^{20} eV and the CMB dominates above 10^{20} eV. The pair creation rate is relevant for Fe energies $4 \cdot 10^{19}$ eV \div $2 \cdot 10^{20}$ eV (γ factors $\sim (1 \div 4) \cdot 10^9$), for which the typical CMB photon energy in the rest frame of the nucleus is above threshold (> 1 MeV) but still well below the peak of the giant resonance ($\sim 10 \div 20$ MeV). The effect of pair creation losses is to reduce the γ factor of the nucleus, obviously leaving A unchanged ⁷.

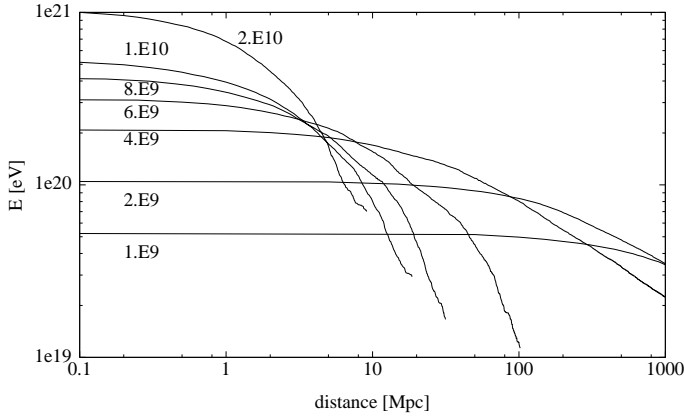


Figure 4: Average energy as a function of the propagation distance for particles that started as Iron nuclei with the indicated Lorentz factors. From Ref. ⁷.

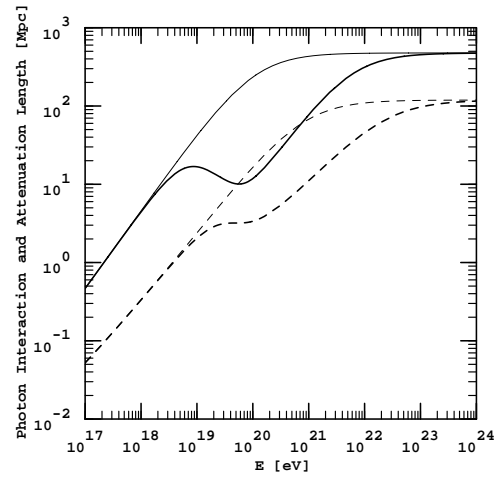


Figure 5: Interaction lengths (dashed lines) and energy attenuation lengths (solid lines) of γ -rays in the CMB (thin lines) and in the combined CMB and URB (thick lines). The interactions taken into account are single and double pair production. From Ref. ⁹.

We should not get fooled by the loss lengths in Fig. 3 into thinking that if the loss length for a Fe nucleus of 10^{20} eV is 500 Mpc, then we can receive on Earth a Fe nucleus that started many hundred Mpc away. This is because the corresponding interaction length is more than an order of magnitude shorter and after every interaction the nucleus becomes lighter and lighter and along with this the loss length for photodisintegration becomes shorter and shorter. The net result ⁷, as can be seen in Fig. 4, is that after 10 Mpc all the energies are below $2 \cdot 10^{20}$ eV and after 100 Mpc they are below 10^{20} eV.

2.3 Photons

As in the case of UHE nucleons and nuclei, the propagation of UHE photons (and electrons/positrons) is also governed by their interaction with the cosmic photon background. The dominant interaction processes in this case are the attenuation of UHE photons due to pair production (PP) on the background photons ($\gamma\gamma_b \rightarrow e^+e^-$), and inverse Compton scattering (ICS) of the electrons (positrons) on the background photons.

The γ -ray threshold energy for PP on a background photon of energy ϵ is

$$E_{\text{thr}} = \frac{m_e^2}{\epsilon} \simeq 2.6 \cdot 10^{11} \left(\frac{\epsilon}{\text{eV}} \right)^{-1} \text{ eV}, \quad (4)$$

whereas ICS has no threshold. In the high-energy limit, the total cross sections for PP and ICS are:

$$\sigma_{\text{PP}} \simeq 2\sigma_{\text{ICS}} \simeq \frac{3}{2}\sigma_{\text{T}}(m_e^2/s) \ln(s/2m_e^2) \quad (s \gg m_e^2). \quad (5)$$

For $s \ll m_e^2$, σ_{ICS} approaches the Thomson cross section $\sigma_{\text{T}} = 8\pi\alpha^2/3m_e^2$ (α is the fine structure constant), whereas σ_{PP} peaks near the threshold. Therefore, the most efficient targets for electrons and γ -rays of energy E are background photons of energy $\epsilon \simeq m_e^2/E$. For UHE this corresponds to $\epsilon \sim < 10^{-6}$ eV $\simeq 100$ MHz. Thus, radio background photons play an important role in UHE γ -ray propagation through extragalactic space ⁹. Unfortunately, the universal radio background (URB) is not very well known, mostly because it is difficult to disentangle the Galactic and extragalactic components.

In the extreme Klein-Nishina limit, $s \gg m_e^2$, either the electron or the positron produced in the process $\gamma\gamma_b \rightarrow e^+e^-$ carries most of the energy of the initial UHE photon. This leading electron can then undergo ICS whose inelasticity (relative to the electron) is close to 1 in the Klein-Nishina limit. As a consequence, the upscattered photon which is now the leading particle after this two-step cycle still carries most of the energy of the original γ -ray, and can initiate a fresh cycle of PP and ICS interactions. This leads to the development of an *electromagnetic (EM) cascade* which plays an important role in the resulting observable γ -ray spectra. An important consequence of the EM cascade development is that the effective penetration depth of the EM cascade, which can be characterized by the energy attenuation length of the leading particle (photon or electron/positron), is considerably greater than just the interaction length (see Fig. 5)⁹.

EM cascades play an important role particularly in some exotic models of UHECR origin such as collapse or annihilation of topological defects in which the UHECR injection spectrum is predicted to be dominated by γ -rays. But, even if only UHE nucleons and nuclei are produced in the first place, for example via conventional shock acceleration, EM cascades can be produced by the secondaries coming from the decay of pions which are created in interactions of UHE nucleons with the low energy photon background¹⁰.

Most of the energy of fully developed EM cascades ends up below ~ 100 GeV where it is constrained by measurements of the diffuse γ -ray flux. Flux predictions involving EM cascades are therefore an important source of constraints of UHE energy injection on cosmological scales.

It should be mentioned that the development of EM cascades depends sensitively on the strength of the extragalactic magnetic fields (EGMFs) which is rather uncertain. The EGMF typically inhibits the cascade development because of the synchrotron cooling of the e^+e^- pairs produced in the PP process. The energy lost through synchrotron radiation does not, however, disappear; rather, it reappears at lower energies and can even initiate fresh EM cascades.

2.4 Neutrinos

The propagation of UHE neutrinos is governed mainly by their interactions with the relic neutrino background (RNB). The interaction energies are typically smaller than electroweak energies even for UHE neutrinos and then the cross sections are given by the Standard Model of electroweak interactions which are well confirmed experimentally. Physics beyond the Standard Model is not expected to play a significant role in UHE neutrino interactions with the low-energy relic backgrounds. Despite the neutrino-neutrino cross section are at least a few order of magnitude smaller than the neutrino-nucleon ones, the latter interactions are negligible compared to interactions with the RNB because the RNB particle density, $\sim 100 \text{ cm}^{-3}$ per family, is about 10 orders of magnitude larger than the baryon density.

The $\nu\bar{\nu}$ annihilation mean free path is of the order of $\lambda_\nu = (n_\nu\sigma_{\nu\bar{\nu}})^{-1} \simeq 4 \cdot 10^{28} \text{ cm}$, just above the present size of the horizon ($H_0^{-1} \sim 10^{28} \text{ cm}$). The neutrino is the only known stable particle that can propagate through the universe essentially uninhibited even at the highest energies. This has led to the speculation that neutrinos could be indeed the super-GZK primaries. However, in the Standard Model a neutrino incident vertically in the atmosphere would pass through it uninhibited, never initiating an extensive air shower. Consequently, for these scenarios to work, one has to postulate new interactions so that these neutrinos acquire a strong cross section above 10^{20} eV .

An interesting situation arises if the RNB consists of massive neutrinos with $m_\nu \simeq 1 \text{ eV}$: such neutrinos would constitute hot dark matter which is expected to cluster, for example, in galaxy clusters. This would potentially increase the interaction probability for any neutrino of energy within the width of the Z^0 resonance at $E = M_Z^2/2m_\nu = 4 \cdot 10^{21} (\text{eV}/m_\nu) \text{ eV}$. It has been suggested that the stable end products of the *Z-bursts* induced at close-by distances

($\sim < 50$ Mpc) from Earth may explain the highest energy cosmic rays¹¹. The problem with these proposals is however that they require a very high flux of UHE neutrinos to begin with and this makes Z-burst above GZK energies more likely to play a role in the context of non-accelerating scenarios. For further information see Ref.⁹ and references therein.

It is important to point out that the only conventional/assured source of UHE neutrinos is the GZK effect itself. The neutrinos are the result of the decay of the pions produced in the $p\gamma$ interaction. The flux however is not very high and the detection is quite difficult. For further informations see Refs.^{9,12}.

3 AGASA and HiRes: is there a discrepancy?

AGASA and HiRes are, up to now, the two experiments with the larger exposure for the detection of UHECRs. They reported however apparently conflicting results. The two reported spectra appear: 1) to have a systematic offset at low energy and 2) to differ above 10^{20} eV where AGASA shown no hint of the GZK-suppression whereas HiRes seems to be consistent with it. It has been shown¹³ that a systematic overestimate of the AGASA energies by 15% and a corresponding underestimate of the HiRes energies by the same amount would in fact bring the two data sets in a much better agreement in the region below 10^{20} eV. In Ref.¹⁴ we applied our Monte Carlo simulation^{13,14,15} to investigate the discrepancies at high energy and we found that:

- assuming a uniform distribution of sources, the AGASA spectrum is reproduced, in a conventional scenario where the average spectrum has the GZK suppression, with a probability of $\sim 6 \cdot 10^{-4}$ ($\sim 3\sigma$).
- assuming the presence of the 15% systematic error, the shifted AGASA data are reproduced with a probability of $\sim 6 \cdot 10^{-3} \div 10^{-2}$ ($2.5\sigma \div 2\sigma$).
- the HiRes data are reproduced, in a scenario without a GZK suppression^a, with a probability of $\sim 2\%$, ($\sim 2\sigma$).

It is important to stress that in order to properly do these calculations one has to take into account the statistical error in the energy determination. Due to the steeply falling spectrum and to the expected change of slope around 10^{20} eV the statistical error in the energy determination changes the average expected number of events above 10^{20} eV by ~ 1 and with the present limited statistics even a difference of one event is important¹⁴.

In Fig. 6 we plot the spectra of some of the simulated AGASA realizations that produced 11 or more events above 10^{20} eV. It is striking the resemblance of the simulated spectra to the AGASA one: all of them show no evidence of the GZK suppression. This shows that the AGASA spectrum is far from being impossible, even if the average cosmic ray spectrum can be expected to show a GZK feature.

From the above points we can conclude that neither AGASA nor HiRes have enough statistical power to prove the presence or absence of the GZK feature in the spectrum of UHECRs. A new generation of experiments is needed to finally provide a conclusive answer to this question.

4 Conclusions

We considered several particles that can possibly play the role of UHECRs and we discussed the energy loss processes that affect their propagation over cosmological distances. We showed that for all considered particles the energy losses above $\sim 10^{20}$ eV become so severe that they cannot propagate over distances larger than about 100 Mpc without reducing their energy below

^aTo mimic a scenario without GZK suppression we used the AGASA dataset as template.

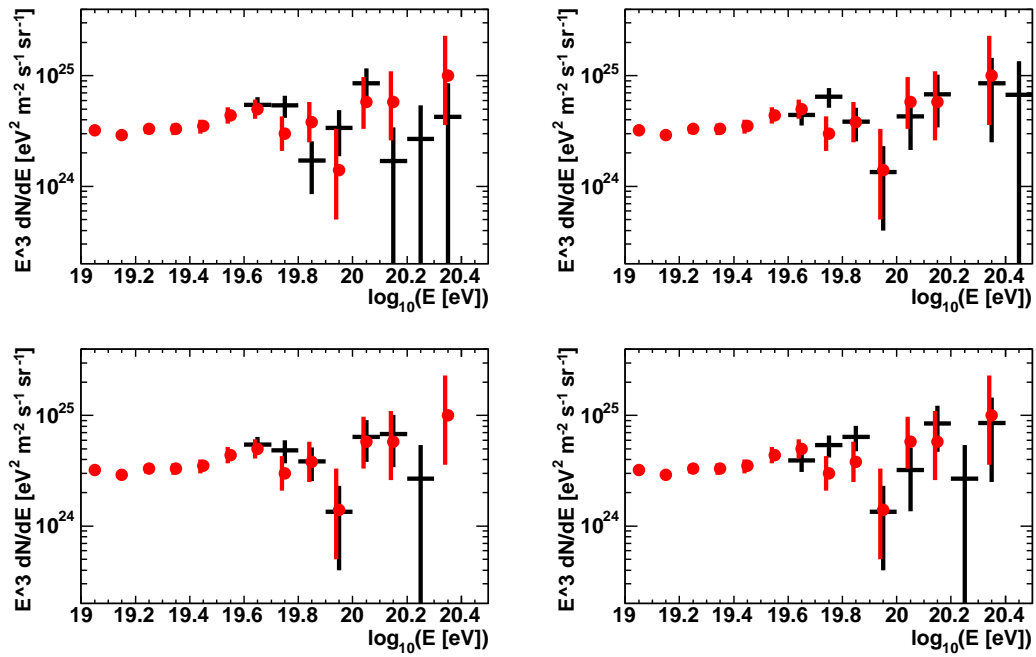


Figure 6: In the above panels we plot 4 of the 18 simulations that have 11 or more events above 10^{20} eV. The black crosses are the simulation results. The red dots with errorbars are the AGASA data superimposed for comparison. The errorbars in the AGASA data are slightly shifted left to avoid covering up the black crosses.

10^{20} eV. The effect of these energy losses on the spectrum of UHECRs is the so called GZK-suppression, due to the fact that below 10^{20} eV almost all the universe is contributing to the observed flux whereas above 10^{20} eV we receive contributions only from sources not too far away, ~ 100 Mpc. We stressed the point that this is not a cutoff, but a *feature* since the spectrum does not end at 10^{20} eV, but it is only suppressed, and the amount of this suppression depends on many unknowns such as: the luminosity evolution of the sources, their local overdensity and the magnetic field strength in the intergalactic medium.

We showed that the present sets of data are not enough to determine whether this GZK suppression is present or not in the observed spectrum and that we need a new generation of experiments to have a conclusive answer to this question.

Acknowledgments

This research is funded in part by NASA grant NAG5-10919.

References

1. K. Greisen, Phys. Rev. Lett. **16**, 748 (1966); G. T. Zatsepin and V. A. Kuzmin, JETP Lett. **4**, 78 (1966).
2. V. S. Berezhinsky and S. I. Grigorjeva, A&A **199**, 1 (1988); V. Berezhinsky, A. Z. Gazizov, and S. I. Grigorjeva, preprint hep-ph/0204357, 2002; Phys. Lett. **B612**, 147 (2005).
3. F. W. Stecker, Phys. Rev. Lett. **21**, 1016 (1968).
4. M. Blanton, P. Blasi, and A. V. Olinto, Astropart. Phys. **15**, 275 (2001).
5. T. Stanev, R. Engel, A. Mücke, R. J. Protheroe, and J. P. Rachen, Phys. Rev. **D62**, 093005 (2000); T. Stanev, D. Seckel, and R. Engel, Phys. Rev. **D68**, 103004 (2003).
6. J. L. Puget, F. W. Stecker, and J. H. Bredekamp, Astrophys. J. **205**, 638 (1976); F. W. Stecker and M. H. Salamon, Astrophys. J. **512**, 521 (1992).

7. L. N. Epele and E. Roulet, *JHEP* **10**, 009 (1998).
8. M. J. Chodorowski, A. A. Zdziarski, and M. Sikora, *Astrophys. J.* **400**, 181 (1992).
9. P. Bhattacharjee and G. Sigl, *Phys. Rept.* **327**, 109 (2000).
10. C. Ferrigno, P. Blasi, and D. De Marco, *Astropart. Phys.* **23**, 211 (2005).
11. T. J. Weiler, *Astropart. Phys.* **11**, 303 (1999); D. Fargion, B. Mele, and A. Salis, *Astrophys. J.* **517**, 725 (1999).
12. R. Engel, D. Seckel, and T. Stanev, *Phys. Rev.* **D64**, 093010 (2001); S. Yoshida and M. Teshima, *Prog. Theor. Phys.* **89**, 833 (1993); F. W. Stecker, *Astrophys. J.* **228**, 919 (1979); S. Yoshida, *Astropart. Phys.* **2**, 187 (1994); C. T. Hill and D. N. Schramm, *Phys. Lett.* **B131**, 247 (1983).
13. D. De Marco, P. Blasi, and A. V. Olinto, *Astropart. Phys.* **20** (2003) 53.
14. D. De Marco, P. Blasi, and A. V. Olinto, in preparation.
15. P. Blasi and D. De Marco, *Astropart. Phys.* **20** (2004) 559.